Received: 06 March 2019 | Revised: 17 June 2019 | Accepted: 21 June 2019

DOI: 10.1002/qj.3599

RESEARCH ARTICLE

Quarterly Journal of the Royal Meteorological Society RMetS

Processes determining heat waves across different European climates

Philipp Zschenderlein[1] | Andreas H. Fink[1] | Stephan Pfahl[2] | Heini Wernli[3]

[1]Institute of Meteorology and Climate Research, Karlsruher Institut für Technologie, Karlsruhe, Germany

[2]Institute of Meteorology, Freie Universität Berlin, Berlin, Germany

[3]Institute of Atmospheric and Climate Science, ETH Zürich, Zurich, Switzerland

Correspondence
Philipp Zschenderlein, Institute of Meteorology and Climate Research, Karlsruher Institut für Technologie, Wolfgang-Gaede-Strasse 1, 76131 Karlsruhe, Germany.
Email: philipp.zschenderlein@kit.edu

Funding information
Funded by the German Research Foundation (DFG);

Abstract

This study presents a comprehensive analysis of processes determining heat waves across different climates in Europe for the period 1979–2016. Heat waves are defined using a percentile-based index and the main processes quantified along trajectories are adiabatic compression by subsidence and local and remote diabatic processes in the upper and lower troposphere. This Lagrangian analysis is complemented by an Eulerian calculation of horizontal temperature advection. During typical summers in Europe, one or two heat waves occur, with an average duration of five days. Whereas high near-surface temperatures over Scandinavia are accompanied by omega-like blocking structures at 500 hPa, heat waves over the Mediterranean are connected to comparably flat ridges. Tracing air masses backwards from the heat waves, we identify three trajectory clusters with coherent thermodynamic characteristics, vertical motions, and geographic origins. In all regions, horizontal temperature advection is almost negligible. In two of the three clusters, subsidence in the free atmosphere is very important in establishing high temperatures near the surface, while the air masses in the third cluster are warmed primarily due to diabatic heating near the surface. Large interregional differences occur between the British Isles and western Russia. Over the latter region, near-surface transport and diabatic heating appear to be very important in determining the intensity of the heat waves, whereas subsidence and adiabatic warming are of first-order importance for the British Isles. Although the large-scale pattern is quasistationary during heat wave days, new air masses are entrained steadily into the lower troposphere during the life cycle of a heat wave. Overall, the results of the present study provide a guideline as to which processes and diagnostics weather and climate studies should focus on to understand the severity of heat waves.

KEYWORDS

adiabatic warming, climatology, diabatic processes, Eulerian perspective, heat waves, Lagrangian perspective

1 INTRODUCTION

Heat waves are very important, due to their various impacts on human health, environment, and economics (Fink *et al.*, 2004; Seneviratne *et al.*, 2012; WMO and WHO, 2015). As a major impact, the human mortality rate is increased during heat events. Xu *et al.* (2016) highlighted that the intensity of heat waves has a higher impact on mortality rates than the duration of the extreme event. Additionally, crop production, ecosystems, and infrastructure are highly influenced by high-temperature events (e.g., Horton *et al.*, 2016). A long-lasting heat and drought period led to wildfires over California in 2017 and cost 13 billion U.S. Dollars in reinsurances (MunichRe, 2018). According to the Fifth Intergovernmental Panel on Climate Change report, the intensity of heat waves in Europe will increase in the future (Collins *et al.*, 2013). Hence, forecasting and assessing the risk of heat waves is a pivotal issue (Messori *et al.*, 2018).

Also, due to the various impacts driven by different characteristics of heat waves, no uniform definition of a heat wave exists (Perkins, 2015). Percentile-based measures are applicable to different climate regions, whereas absolute temperatures are more suitable for assessing societal impacts (e.g., Horton *et al.*, 2016). In our study, we use the Heat Wave Magnitude Index daily (HWMId) of Russo *et al.* (2015), which is a percentile-based metric that combines multiple heat wave characteristics and is able to identify the severe heat waves that typically occur in the summer season.

Summertime warm temperature extremes over mid- to high-latitude land regions are related to co-located blocking high-pressure systems (Pfahl and Wernli, 2012; Stefanon *et al.*, 2012; Pfahl, 2014; Sousa *et al.*, 2018; Woollings *et al.*, 2018), which interrupt the prevailing westerlies in the Northern Hemisphere (Tyrlis and Hoskins, 2008). Schaller *et al.* (2018), using large climate model ensembles, demonstrated that the relation between heat waves and blocking will not be modified in the future. Additionally to the blocking pattern, a deep trough covering the North Atlantic Ocean with a ridge downstream over the European continent can lead to warm air-mass advection from northern Africa and the Mediterranean basin (Cassou *et al.*, 2005). Other studies emphasized the advection of hot and dry air masses from the south leading to high temperatures during heat waves in Europe (Miralles *et al.*, 2014) and the Northern Hemisphere in general (Perkins, 2015). For Australian heat waves, Boschat *et al.* (2015) highlighted warm-air advection from the inner Australian continent. In the upper troposphere, large-amplitude noncircumglobal Rossby-wave packages (RWPs) are linked to temperature extremes at lower levels (Fragkoulidis *et al.*, 2018; Wirth *et al.*, 2018). As an example, RWPs originating from western North America propagated towards Europe, became stationary, and attained larger amplitudes and coincided with a heat wave in the late summer of 2016 (Zschenderlein *et al.*, 2018). Also, circumglobal jet waviness is linked to temperature extremes (Petoukhov *et al.*, 2013), although to a lesser extent compared with noncircumglobal waviness (Röthlisberger *et al.*, 2016; Fragkoulidis *et al.*, 2018).

During periods of high soil-moisture content, latent heat fluxes exceed the surface sensible heat fluxes. During dry soil periods, which are more typical during heat waves, surface sensible heat fluxes are crucial (Alexander, 2011). Due to the lower soil and vegetation moisture content, land evaporation decreases and the enhanced sensible heat fluxes associated with such land–atmospheric feedbacks can increase maximum temperatures (Fischer *et al.*, 2007; Hirschi *et al.*, 2011; Miralles *et al.*, 2014; Miralles *et al.*, 2019).

Studying temperature extremes with Lagrangian trajectories gives insight into source regions, typical transport patterns, and physical processes in the air masses (Bieli *et al.*, 2015; Santos *et al.*, 2015; Quinting and Reeder, 2017; Zschenderlein *et al.*, 2018). Bieli *et al.* (2015) focused on high- and low-temperature extremes in three European regions, regardless of their duration, and showed that high-temperature events are generally associated with weaker horizontal transport than cold temperature events, but they experience strong adiabatic warming by subsidence and enhanced surface radiation and surface fluxes. Santos *et al.* (2015) studied temperature extremes occurring in different seasons over the Iberian Peninsula, noting the importance of the Iberian heat low in summer and the significant contribution of air-parcel descent, radiative cooling in the free atmosphere, and near-surface warming. Lee and Grotjahn (2016) employed backward trajectories and showed that adiabatic heating and horizontal advection were the main factors in determining the anomalous high temperatures in the lower troposphere above California. A study focusing on heat waves in southeastern Australia emphasized the role of adiabatic compression and de-emphasized the role of local surface fluxes (Quinting and Reeder, 2017).

The Eulerian temperature tendency equation states that temperature can increase due to three different processes: horizontal advection, adiabatic compression due to vertical motion, and diabatic processes (Carlson, 1994). Our aim is to quantify which process dominates in establishing near-surface high-temperature extremes across different European climates. To this end, we trace the air masses associated with heat waves in Europe backward in time, similar to Bieli *et al.* (2015). In contrast to Bieli *et al.* (2015), we focus only on heat waves with a minimum duration of three days in six European regions, including regions that were not yet studied with Lagrangian trajectories so far, that is, western Russia and Scandinavia. We analyse source regions, typical pathways, and the physical processes along the trajectories. Furthermore, we identify trajectory clusters with unique coherent

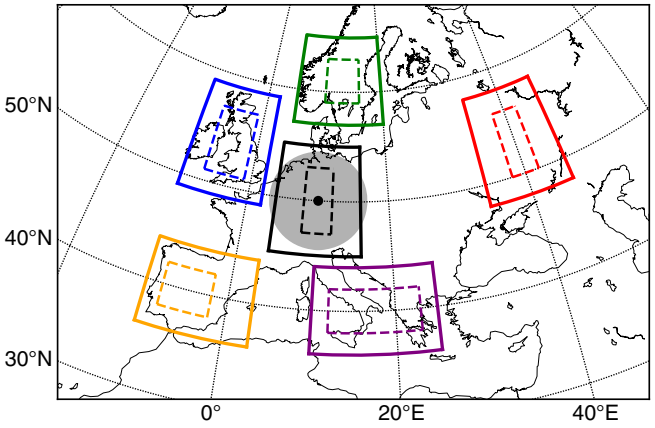

FIGURE 1 Regions studied in Europe: Scandinavia (green; solid box: 57°N–65°N, 5°E–20°E; dashed box: 59°N–63°N, 10°E–16°E); western Russia (red; solid box: 48°N–58°N, 34°E–46°E; dashed box: 50°N–56°N, 38°E–42°E); Greece/Italy (purple; solid box: 36°N–44°N, 10°E–25°E, dashed box: 38°N–42°N, 12°E–23°E); Iberian Peninsula (orange; solid box: 36°N–44°N, 10°W–3°E; dashed box: 38°N–42°N, 8°W–2°W); British Isles (blue; solid box: 49°N–59°N, 10°W–2°E; dashed box: 51°N–57°N, 8°W–1°W), and Central Europe (black; solid box: 45°N–55°N, 4°E–16°E, dashed box: 47°N–53°N, 8°E–12°E). The solid lines represents the regions employed for the backward trajectories, the dashed lines are the borders for the forward trajectories. The grey circle (exemplarily shown for Central Europe) with a radius of 500 km is used for calculation of the residence time; see also section 2.2

thermodynamic processes and vertical motions. Additionally, we diagnose typical geopotential height patterns during the onset of heat waves. Finally, we quantify how long air parcels reside in the target area to answer the question of whether heat waves are influenced steadily by new air masses or whether the air parcels are being stalled in the lower troposphere over a longer time period.

Section 2 provides an overview of the data and methods employed in this study. The results in section 3 include the typical durations and frequencies of heat waves, as well as their onset patterns. The clustering of the trajectories, the source regions, and the physical processes along the trajectory clusters are discussed. After that, we quantify how long the trajectories stay in the target region. Section 4 closes with a summary of the main results and avenues for further research.

2 | DATA AND METHODS

2.1 | Heat wave identification

Heat waves are analysed with the ERA-Interim reanalysis product (Dee *et al.*, 2011) of the European Centre for Medium-Range Weather Forecasts (ECMWF). The reanalysis contains temperatures at 2 m height and we use a horizontal resolution of 1° × 1° for the time steps 0000, 0600, 1200, and 1800 UTC during 1979–2016.

The identification of heat waves consist of three steps. Firstly, we define the study regions in Europe (Figure 1), with the aim of reflecting and comparing the different climates in Europe. Most of the regions are defined following Bieli *et al.* (2015) and Santos *et al.* (2015). The other regions are chosen in order to complement the different European climates. The position of the easternmost region is motivated by the position of extreme heat wave in 2010 over western (Grumm, 2011).

Secondly, we identify the heat wave occurrences in these regions. For that, we calculate the percentile-based HWMId (Russo *et al.*, 2015). According to Russo *et al.* (2015), a heat wave is defined as a period of at least three consecutive days with a daily maximum temperature above a threshold. This threshold is defined as the 90th percentile of the daily maximum of 0000, 0600, 1200, and 1800 UTC temperatures at 2 m height within a centred 31-day window in the years 1979–2016. This approach identifies heat waves in all seasons. As an example, to calculate the 90th percentile on August 16, we consider the grid-point daily maximum temperature values between August 1 and 31 for the 38 years between 1979 and 2016.

The second part of the HWMId filters the stronger heat waves that usually occur during summer, that is, June, July, and August in the Northern Hemisphere. The daily heat wave magnitude M_d is defined as

$$M_d = \begin{cases} \dfrac{T_d - T_{30y25p}}{T_{30y75p} - T_{30y25p}} & \text{if } T_d > T_{30y25p}, \\ 0 & \text{if } T_d \leq T_{30y25p}, \end{cases} \quad (1)$$

with T_d being the maximum of 0000, 0600, 1200, and 1800 UTC 2-m temperature and T_{30y75p} (T_{30y25p}) the 75th (25th) percentile of annual maximum temperatures between 1979 and 2016. The criterion $T_d > T_{30y25p}$ identifies heat waves in the warmest time of the year, usually during June, July, and August (JJA). Hence, all heat waves identified with $M_d > 0$ occur during the summer season. Thirdly, we want to exclude very small areas of high-temperature extremes, because heat waves are typically a synoptic-scale phenomenon (Stefanon *et al.*, 2012). As a consequence, we define that at least 5% of the predefined region (Figure 1) should exceed $M_d > 0$ per day to be identified as a heat wave. As a result of the three identification steps, we deduced a heat wave list for every region that serves as our heat wave climatology.

We now briefly present an example of the heat wave identification. After the first identification step, namely the definition of the study region, the heat wave occurrence has to be defined. Figure 2 depicts the fraction of the study region exceeding the 90th percentile of daily maximum temperatures and the 25th percentile of the annual maximum temperatures in order to fulfil Equation 1. The HWMId requires that at least three consecutive days must exceed these thresholds. Our

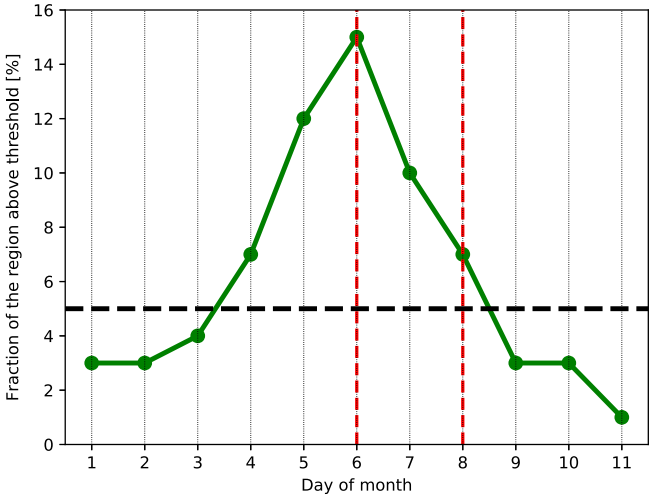

FIGURE 2 Example of heat wave identification showing a time series of the area exceeding the 90th percentile of 2-m daily maximum temperature and 25th percentile of annual maximum 2-m temperature. The black dashed line shows the minimum area to be defined as a heat wave, the vertical red dashed lines show the start and end of the heat wave. For further information, see text

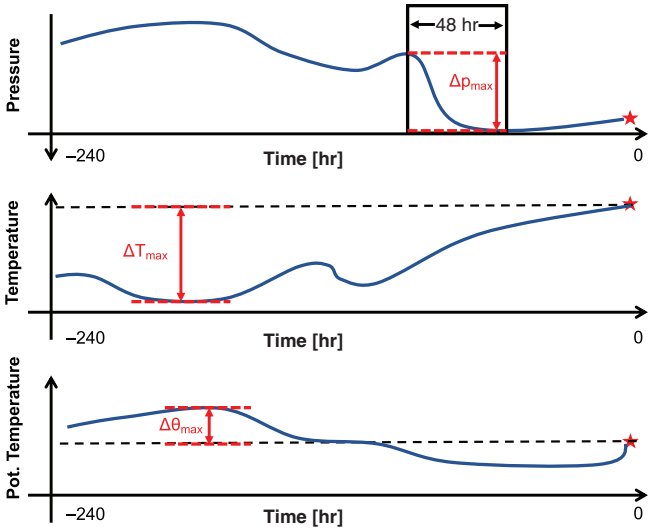

FIGURE 3 Schematic describing the three properties used for the clustering of trajectories. The three diagrams show the temporal evolution of temperature (T), pressure (p), and potential temperature (θ) along one backward trajectory, which has its starting point at the red star. The three red-marked properties $\Delta p_{\max}$, $\Delta T_{\max}$, and $\Delta\theta_{\max}$ will be used for the clustering described in Table 1. For further explanations, see text

additional requirement is that at least 5% of the study region must exceed these thresholds. In the example in Figure 2, the days between the fourth and the eighth of the month exceed both thresholds in at least 5% of the study region. However, the heat wave starts only on the sixth, because this day is the first day when at least three consecutive days fulfil all requirements. Hence, the heat wave lasts three days, from the sixth to the eighth of the month, which is the shortest possible duration of a heat wave. Thus, we slightly modified the application of the HWMId. The heat wave duration is not assessed based on single grid points, but on larger areas in which at least 5% of the area exceeds both the 90th percentile of daily maximum temperature and the 25th percentile of annual maximum temperature in a given day. In Russo *et al.* (2015), a heat wave duration was calculated by the number of days that exceeded the first threshold.

2.2 | Trajectory calculation

We compute 10-day backward trajectories with Lagrangian analysis tool (LAGRANTO) (Sprenger and Wernli, 2015), which are driven by six-hourly ERA-Interim three-dimensional wind fields on a 1° × 1° latitude/ longitude grid and 60 vertical model levels. Trajectories are started for every heat wave day at 1200 UTC. Throughout the study, we use the following terminology concerning the backward trajectories: the starting point of a trajectory is the grid point where it was initialized in the heat wave region (e.g., a grid point in Central Europe). The endpoint of the trajectory (10 days before the start) is denoted as the origin, or the source. The first seven days refer to the period between ten and three days before their arrival in the target area. In order to understand the build-up of the near-surface heat, trajectories are started at 10, 30, 50, and 100 hPa above ground level. We exclude starting points above sea surfaces. Furthermore, the following variables are traced along the trajectories: pressure (p), temperature (T), potential temperature (θ), relative humidity (rh), specific humidity (q), and six-hourly accumulated surface sensible heat fluxes ($sshf$).

For each trajectory, we aim to quantify the overall temperature and potential temperature changes and relate these changes to vertical motions. For that, we use the approach of Binder *et al.* (2017) and calculate the maximum changes of temperature and potential temperature, as well as maximum pressure increases, that is, descents, along all trajectories. More precisely, we calculate for both T and θ the maximum absolute difference between the respective value at the starting point of the trajectory and the previous time steps. The outcome of this method is referred to as $\Delta T_{\max}$ and $\Delta\theta_{\max}$, respectively (Figure 3). In order to relate these changes to the descent of the air parcels, we also calculate the maximum pressure increase in all 48-hr windows along the trajectories (Figure 3). Accordingly, the outcome of this method is referred to as $\Delta p_{\max}$. These three values allow us to sort the trajectories into different categories with different thermodynamic characteristics: (a) positive $\Delta T_{\max}$ and negative $\Delta\theta_{\max}$ (cluster A) , (b) both positive $\Delta T_{\max}$ and $\Delta\theta_{\max}$ (cluster B), (c) negative $\Delta T_{\max}$ and positive $\Delta\theta_{\max}$ (cluster C), and (d) both negative $\Delta T_{\max}$ and $\Delta\theta_{\max}$ (cluster D). Assuming a surface pressure of 1000 hPa, the starting points of the trajectories are defined at 990, 970, 950, and 900 hPa. Hence, a maximum pressure increase of 100 hPa in 48 hr for air parcels starting at 900 hPa would imply a level of around 800 hPa

TABLE 1 Definitions of the trajectory clusters; bold marked clusters are discussed in the study. ΔT_{max}, $\Delta\theta_{max}$, and Δp_{max} are described in section 2.2 and Figure 3. For further information, see text

Cluster	ΔT_{max}	$\Delta\theta_{max}$	Δp_{max} in 48 hr
A	>0	<0	Not considered
$\boldsymbol{B}_{sd}$	>0	>0	>100 hPa
$\boldsymbol{B}_{wd}$	>0	>0	≤100 hPa
C	<0	>0	Not considered
D	<0	<0	Not considered

as maximum height, when the ascension starts directly from 900 hPa. In that case, the air parcel is still in the lower troposphere. In addition to the thermodynamic characteristics, we can therefore subdivide each cluster into trajectories with strong descent, that is, more than 100 hPa in 48 hr, and weak descent, that is, less than 100 hPa in 48 hr. The choice of the 100 hPa threshold is subjective, but the results in section 3.3 justify this threshold. Section 3.3 shows that the subdivision into strong and weak descent is mainly important for cluster *B*. Table 1 summarizes the characteristics of the different clusters. This physical clustering is very useful in quantifying the relative roles of subsidence and diabatic processes in shaping near-surface high-temperature extremes.

In order to identify the residence time of air parcels in the regions defined in Figure 1, we calculate forward trajectories for all identified heat wave days. The residence time is defined as the time period between the start of the trajectories and the first time exiting the region. Due to the different sizes of the solid boxes in Figure 1, we define the region as a circle with a fixed radius of 500 km. The centre of the circle is located in the middle of each solid box, as exemplarily shown for Central Europe in Figure 1. A radius of 500 km is chosen because the regions have a size of roughly $900 \times 900\,km^2$. Forward trajectories starting near the border of the region may have very short residence times. To avoid these cases, we reduce the amount of initialization points of the forward trajectories to the dashed rectangles inside our regions (Figure 1). As an example, we initialize the forward trajectories for Central Europe only between 47° and 53°N and 8° and 12°E, and quantify the duration air parcels need to leave the circle with its centre at 50°N and 10°E.

3 | RESULTS

The following section first gives a statistical overview of the heat waves identified, followed by the typical 500-hPa geopotential height onset patterns. Subsequently, the origin of the trajectories and the associated processes are presented.

3.1 | Heat wave statistics

Typically, in each region one or two heat waves occur during a year (Figure 4a). The variability of occurrence is largest in western Russia, presumably due to the continental climate. Maximum numbers of heat waves per year range between five and eight. It is possible that two heat waves are only interrupted by one day, although this is very rare. The extreme summer of 2003, which mainly affected Central Europe (Fink *et al.*, 2004), consists of five heat waves, each with different lengths (Figure S1). The most intense one occurred during the first half of August 2003 (Table S1). Hence, the accumulation of several heat waves can lead to an overall extreme summer. Regions under maritime influence, that is, Greece/Italy, the Iberian Peninsula, and the British Isles have some years with no heat wave, presumably due to the generally lower climate variability in the maritime regions. Additionally, it is also possible that extreme hot days occur on a smaller scale in the maritime regions.

Throughout the different regions, on average 5–10 heat wave days occur per year (Figure 4b). The annual maximum of heat wave days ranges between 25 days for Scandinavia and nearly 60 days for western Russia. Similar to the heat wave occurrence, the highest variability is found for western Russia. The maximum numbers of heat wave days, about 60 in western Russia and 30 in Central Europe, concur with the extreme heat waves in 2010 (Grumm, 2011; Quandt *et al.*, 2017) and 2003 (Fink *et al.*, 2004), respectively (Figures S1 and S2).

Figure 4c presents the typical duration of heat waves in Europe. By construction, the minimum duration is three days and the median duration ranges between four and five days. The median duration is similar to the typical minimum duration of atmospheric blocking, which often coincides with high temperatures in summer (Pfahl and Wernli, 2012). Most of the heat waves last between three and seven days, while durations above 10 days are rare. A maximum duration of 44 days in western Russia is noteworthy because of its extreme length. In fact, the 44 days refers to the 2010 extreme heat wave in Russia, which had large impacts. The maximum duration of heat waves in Central Europe is 13 days, over the British Isles and Scandinavia 12 days, over the Iberian Peninsula 17 days, and in Greece/Italy 10 days, respectively.

The heat wave durations are similar to those in Stefanon *et al.* (2012) and Perkins *et al.* (2012). Fischer and Schär (2010) defined heat waves with a minimum duration of six days and obtained generally longer heat waves, but with a decreased occurrence probability compared with our results.

The HWMId can be used for a ranking of the most intense heat waves in the different regions. As a result, the two most intense heat waves in Central Europe occurred in 2003 and 2015 (Table S1), in Scandinavia in 1991 and 2014 (Table S2), in western Russia in 2010 and 1981 (Table S3), in Greece/Italy in 2007 and 1988 (Table S4), in the Iberian Peninsula in 1982 and 2015 (Table S5), and in the British Isles in 1990 and 2006 (Table S6). Interestingly, no year features

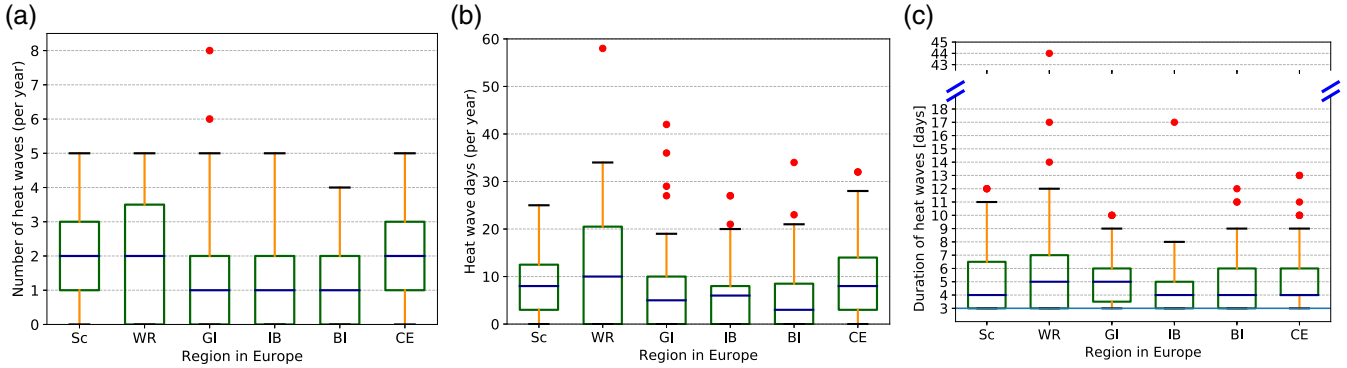

FIGURE 4 A statistical overview of the heat waves identified in Scandinavia (Sc), western Russia (WR), Greece/Italy (GI), Iberian Peninsula (IB), British Isles (BI), and Central Europe (CE). The box plots in (a) depict the numbers of heat waves per year, (b) shows the number of heat wave days per year, and (c) illustrates the duration of the heat waves. Note the cut *y*-axis in (c). Blue horizontal lines denote the median, the boxes the interquartile range, the whiskers 1.5 times the interquartile range, and the red dots the outliers

the most intense heat wave in more than one region, indicating that extreme heat waves rarely extend over our defined regions.

3.2 | Onset pattern

This section analyses composites of 500-hPa geopotential height onset patterns during the onset of heat waves in Europe. We define the onset as the first day of a heat wave (left dashed red line in Figure 2). In all regions, upper-level ridges are colocated with the onset of heat waves (Figure 5), corroborating the findings of Pfahl and Wernli (2012) and Sousa *et al.* (2018). The variability of the geopotential height in the area of the ridges is low compared with the regions upstream, polewards and downstream of the heat waves. Although the ridge pattern is similar for the individual heat waves, the amplitude of the upstream trough is more variable.

The shape of the ridge over Scandinavia resembles an omega-like blocking structure associated with a dominant interruption of the westerlies (Figure 5b), whereas ridges over Central Europe (Figure 5c), the British Isles (Figure 5a), and western Russia (Figure 5d) do not have this pronounced omega shape. Ridges in southern Europe over Greece/Italy (Figure 5f) and the Iberian Peninsula (Figure 5e), however, are much less pronounced. In fact, those ridges are comparably flat. Thus, heat waves in southern Europe occur while other regions in Europe are under influence of nearly zonal weather regimes. Composites by definition average over many patterns, which means that individual cases can have different trough–ridge configurations. Sousa *et al.* (2018) emphasized that it is important to differentiate between classical high-latitude blocking and subtropical ridges when investigating the relationship to heat events in Europe. The authors argued that classical European blocking configurations are not associated with heat waves over more southerly latitudes, which often experience negative temperature anomalies during blocking episodes. Those negative temperature anomalies can be explained by the troughs at the eastern and western flanks of the blocking over Scandinavia (Figure 5b).

Comparing the synoptic patterns for the European regions reveals some interesting interregional relations. A simultaneous heat wave over the British Isles and Scandinavia is improbable, because the ridges are too narrow (Figure 5a,b), although it should be noted that during the strong heat wave in 2018 both regions featured a simultaneous heat wave (not shown). Furthermore, the synoptic patterns are nearly zonal in most parts of Europe under heat wave conditions in western Russia (Figure 5d). This is also the reason why, during the extreme heat wave in 2010 over western Russia, the rest of Europe was hardly affected by heat waves (Figure S2). Of course, these patterns are very variable from case to case, but, overall, it can be concluded that heat waves in Europe are affected by upper-level ridges with a zonal extension of $<$ 2,000 km and a varying amplitude, depending on the latitude of the affected region.

3.3 | Trajectory clusters

After applying the method described in section 2.2 (see also Figure 3) to the heat wave trajectories in each region, each trajectory, according to its values of $\Delta T_{\max}$, $\Delta\theta_{\max}$, and $\Delta p_{\max}$, can be associated with one of the five different clusters (see Table 1 for the definition of the clusters). As an example, we show the outcome of this procedure for Central Europe in Figure 6a. The diagrams of $\Delta T_{\max}$, $\Delta\theta_{\max}$, and $\Delta p_{\max}$ for the other European regions are shown in Figures S3–S7. Obviously, no trajectories can be found on or near the axes, because the maximum changes of both T and θ were calculated. A trajectory on the axes would imply that either T or θ would be strictly constant throughout the whole 10-day period, a situation that does not exist in the real atmosphere.

About one quarter of all trajectories creating a heat wave in Central Europe belong to cluster *A* (upper left quadrant in Figure 6a). Air parcels in this cluster experience an overall

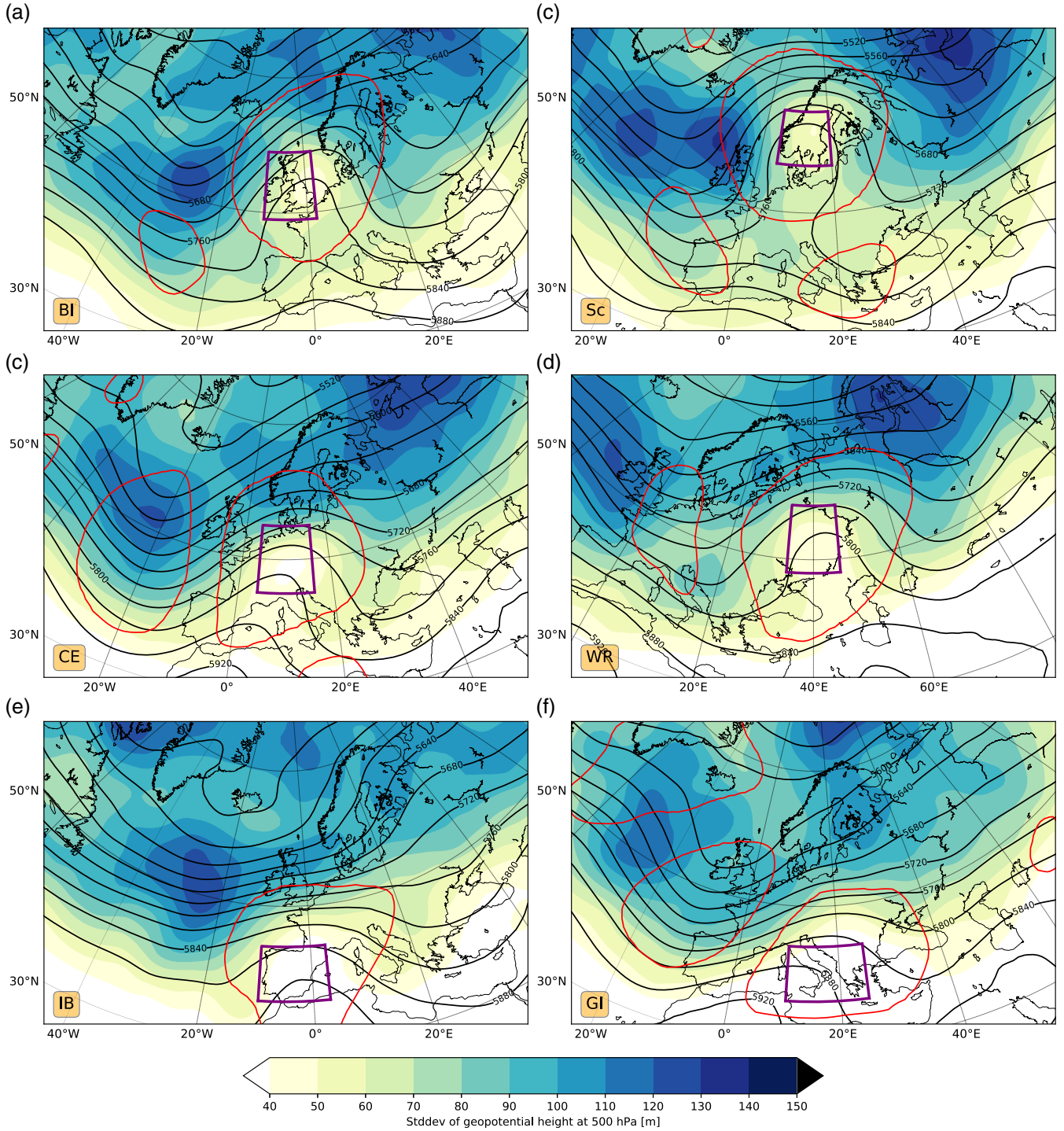

FIGURE 5 Geopotential height patterns during the onset of heat waves in different regions in Europe: (a) British Isles (BI, see box in bottom left corner), (b) Scandinavia (Sc), (c) Central Europe (CE), (d) western Russia (WR), (e) Iberian Peninsula (IB), and (f) Greece/Italy (GI). The contours depict the mean and colours the standard deviation over all events for the 500-hPa geopotential height (in m). Areas surrounded by red lines indicate significance at the 1% level based on a Student's *t*-test

diabatic cooling of up to −20 K and at the same time a temperature increase of up to +80 K during the 10-day period. This is possible due to subsidence, which leads to adiabatic warming overcompensating the diabatic cooling of the air parcels. Hence, stronger subsidence is accompanied by higher temperature increases. The diabatic cooling during the subsidence in the free atmosphere is presumably due to radiative cooling (Bieli *et al.*, 2015; Binder *et al.*, 2017; Raveh-Rubin, 2017).

Trajectories in the upper right quadrant of Figure 6a comprise roughly three-quarters of all trajectories establishing a heat wave in Central Europe. Similar to cluster *A*, air parcels experience a maximum temperature increase of up to

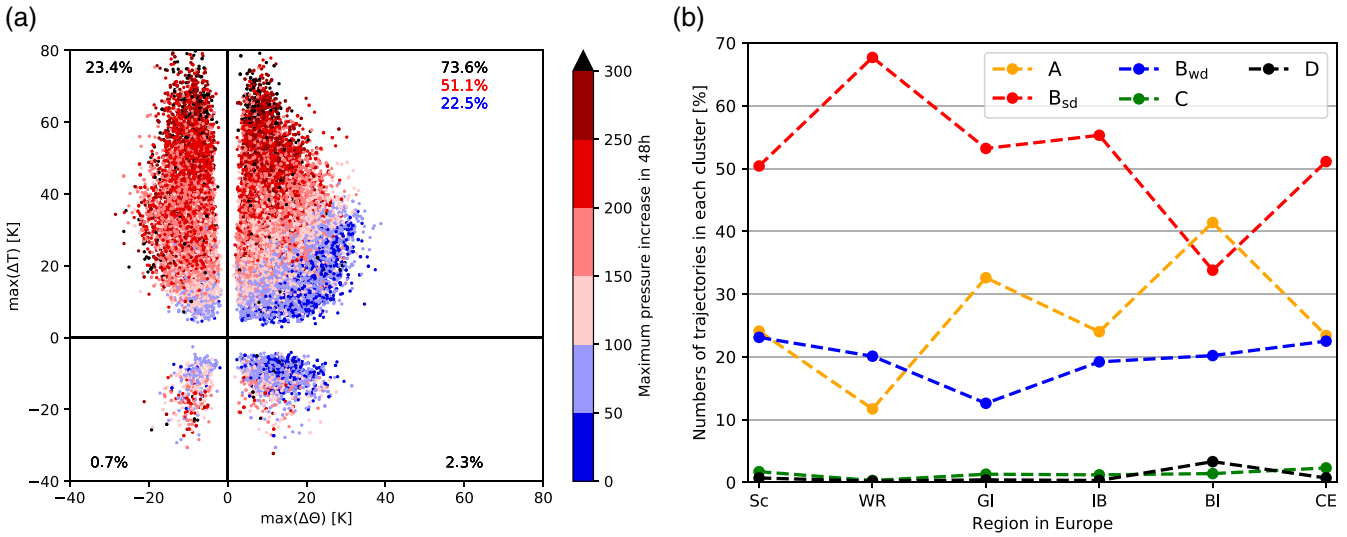

FIGURE 6 Thermodynamic changes for the trajectory clusters. (a) Maximum temperature (ΔT_{max}, in K) and maximum potential temperature ($\Delta\theta_{max}$, in K) changes along the trajectories for heat waves in Central Europe. The colours indicate the maximum pressure increase in a 48-hr window. The numbers in the quadrants denote the fraction of trajectories in each cluster: in black (irrespective of descent rate), blue (descent ≤100 hPa in 48 hr, only upper right quadrant), and red (descent >100 hPa in 48 hr, only upper right quadrant). Additionally, the letters in boxes indicate the names of the clusters and the black sloping line denotes the approximate border between clusters B_{sd} and B_{wd}. (b) Fraction of trajectories in clusters for all investigated regions in Europe (Sc: Scandinavia, WR: western Russia, GI: Greece/Italy, IB: Iberian Peninsula, BI: British Isles, CE: Central Europe)

+80 K, but, in contrast to cluster *A*, air parcels are diabatically warmed by up to +40 K. The trajectories in the upper right quadrant of Figure 6a can be subdivided into two clusters: air parcels descending more than 100 hPa in 48 hr (red colours in Figure 6a and defined as cluster B_{sd} for strong descent) and those descending less than 100 hPa in 48 hr (blue colours in Figure 6a and defined as cluster B_{wd} for weak descent). Compared with B_{sd}, trajectories in cluster B_{wd} exhibit lower temperature increases, but to some extent higher maximum diabatic heating. As a result, air parcels in B_{wd} are mainly warmed due to diabatic heating in the absence of strong vertical motion, whereas air parcels in B_{sd} are warmed due to the combination of strong subsidence and diabatic heating near the surface.

Trajectories in the lower right quadrant of Figure 6a experience an overall temperature decrease and diabatic heating (cluster *C*) and trajectories in the lower left quadrant of Figure 6a are also cooled overall, but they are diabatically cooled (cluster *D*). Comparing the numbers of trajectories of clusters *C* and *D* with those of the abovementioned clusters *A*, B_{sd}, and B_{wd}, it is found that they are negligible; they are therefore not discussed further.

As we have shown, mainly three trajectory clusters with coherent thermodynamic characteristics and vertical motions create heat waves in Central Europe. In the other European regions, clusters *C* and *D* are negligibly small (Figure 6b) as well. However, the other three clusters *A*, B_{sd}, and B_{wd} all contribute to heat waves, with varying importance depending on the region. In most of the regions, 50% of the trajectories are in cluster B_{sd}, but the largest differences are found for western Russia and the British Isles. Western Russia is strongly influenced by cluster B_{sd} (about 70%), that is, a combination of subsidence and diabatic heating, and less influenced by cluster *A* (about 10%), hence the majority of the air parcels are diabatically heated. The British Isles have the largest portion of trajectories in cluster *A* (about 40%) compared with the other regions, where between 25 and 30% of the trajectories fall into cluster *A*. The fraction of cluster B_{wd} does not vary that much between the regions—only Greece/Italy show a smaller fraction. Possible causes for the interregional differences are discussed in the next sections.

3.4 | Physical processes along the trajectory clusters

Figure 7 depicts the source regions three and seven days prior to the heat waves. Seven days prior to the heat waves, air parcels often originate from the west, that is, above the North Atlantic Ocean, which is reasonable given the climatic westerly flow towards Europe. Western Russia is the only exception, because it is partly beyond the direct reach of the jet stream and systems of North Atlantic origin. Here, trajectories originate mostly over the Eurasian continent and less over the North Atlantic Ocean. For heat waves in Scandinavia, nearly no trajectory originates in the Mediterranean, which suggests that warm-air advection from typically warm regions is of minor importance for heat waves in Scandinavia. It is therefore also possible that air parcels originate from climatologically cold areas polewards of the polar circle and later

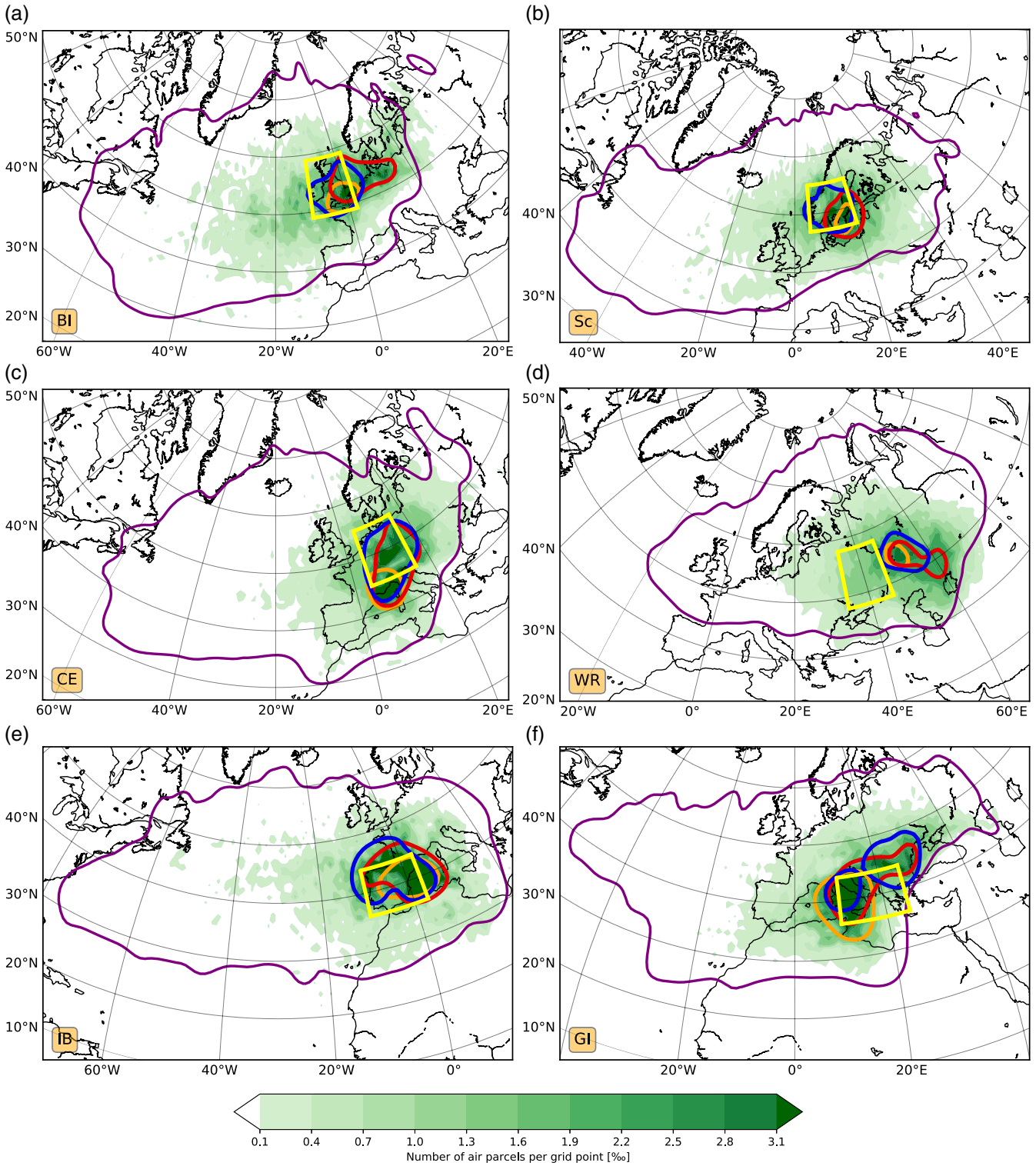

FIGURE 7 Spatial distribution of trajectories. The purple line represents the fraction of air parcels per grid point of at least 0.1‰ seven days prior to the heat waves, irrespective of the clusters. The green colour shading represents the position of air parcels three days prior to arrival in the heat wave regions: (a) British Isles, (b) Scandinavia, (c) Central Europe, (d) western Russia, (e) Iberian Peninsula, and (f) Greece/Italy. The orange line represents the fraction of trajectories per grid point of at least 2.2‰ for cluster A, the red line similarly for cluster B_{sd} and the blue line similarly for cluster B_{wd} three days prior to the heat waves

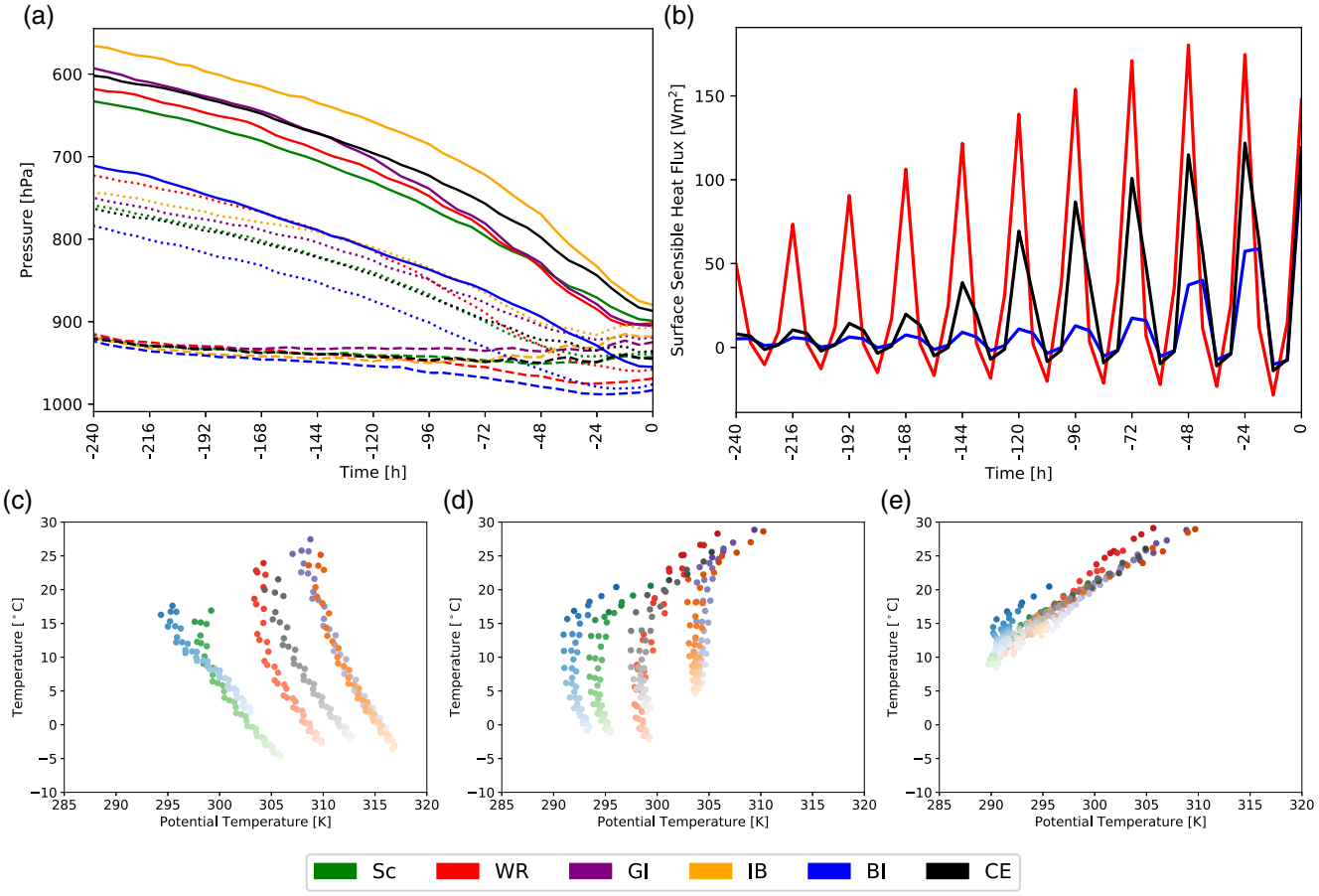

FIGURE 8 Processes along the trajectories for Scandinavia (Sc), western Russia (WR), Greece/Italy (GI), Iberian Peninsula (IB), British Isles (BI), and Central Europe (CE). (a) Temporal evolution of median pressure for the three trajectory clusters: A (solid), B_{sd} (dotted), and B_{wd} (dashed). (b) Surface sensible heat fluxes (median) for trajectories in clusters B_{sd} and B_{wd} together, but with the additional constraint of being located between the surface and 850 hPa. For better visibility, we only show three regions that represent typical characteristics. (c–e) T–θ diagrams illustrating the temporal evolution of (median) temperature and potential temperature for the three trajectory clusters (c) A, (d) B_{sd}, and (e) B_{wd}. Darker colours denote time steps closer to the heat wave

contribute to the heat wave. Our results are in marked contrast to the view that heat waves in Europe are associated with warm-air advection from southerly regions (for example, Perkins, 2015; Miralles *et al.*, 2014). Hence the (Lagrangian) processes in the air parcels seem to be very important for establishing high temperatures near the surface, as discussed in the following.

Air parcels in trajectory cluster A originate from the highest altitudes (Figure 8a) and descend with a similar rate 10–5 days prior to the heat waves. In the second five days, the rate of descent increases, particularly for Greece/Italy, western Russia, and the Iberian Peninsula, before the air parcels are entrained into the planetary boundary layer. The subsidence in the free atmosphere concurs with radiative cooling in all regions (Figure 8c). Although the air parcels are diabatically cooled, their temperature increases (Figure 8c) because the subsidence leads to adiabatic warming, which overcompensates the diabatic cooling. Interestingly, temperatures in the source region of cluster A arriving in Greece/Italy, Central Europe, western Russia, and the Iberian Peninsula are colder than those for the British Isles, but the temperatures near the surface are higher for the four former regions, highlighting the importance of subsidence. As mentioned by Bieli *et al.* (2015), temperature extremes develop on a time-scale between two and three days. Figure 7 therefore shows the position of the three clusters three days prior to the heat waves. Most of the trajectories in cluster A are already located in the target region in the last three days. Western Russia is the only exception, where cluster A is located to the east of the target area. Air masses seem to be trapped in the target regions while descending. Hence subsidence above the target area or in the vicinity is essential in determining the extreme temperatures near the surface for cluster A.

Air parcels in trajectory cluster B_{sd} descend 10–2 days before their arrival in the heat wave regions, similarly to cluster A, but with the difference that B_{sd} trajectories enter the planetary boundary layer earlier (Figure 8a). In the free atmosphere, subsidence is associated with weak radiative cooling or is nearly adiabatic for B_{sd} trajectories arriving

in Greece/Italy and the Iberian Peninsula (Figure 8d). During the last 72 hr, B_{sd} trajectories were warmed diabatically near the surface (Figure 8d). Air parcels in trajectory cluster B_{wd} remain in the lower troposphere around 950 hPa over the whole 10 days (Figure 8a) and are continuously warmed diabatically (Figure 8e). The quasilinear relationship between temperature and potential temperature increase in this cluster suggests that the air parcels are warmed only due to diabatic processes. While the origin temperatures of cluster B_{wd} are higher compared with the other two clusters, the overall temperature increase is smaller, due to the missing subsidence.

Increased solar radiation during clear-sky conditions leads to an increase of surface sensible heat fluxes (Alexander, 2011), thus warming the air parcels near the surface diabatically. It is therefore interesting to look at the trajectories that are heated diabatically and located near the surface. Figure 8b illustrates the temporal evolution of the median of the surface sensible heat fluxes for clusters B_{sd} and B_{wd} together. Because surface sensible heat fluxes are, by definition, only effective in the lower troposphere, the surface sensible heat fluxes in Figure 8b are only shown for trajectories located between the surface and 850 hPa.

Air parcels contributing to a heat wave in western Russia are strongly influenced by surface sensible heat fluxes in the last three days before the onset of the heat wave, with maximum values around 175 W/m^2. Even up to seven days prior to the heat waves, air parcels located near the surface are influenced by diabatic heating above 100 W/m^2. Indeed, trajectories in clusters B_{sd} and B_{wd} are located to the east of western Russia and above land surfaces (Figure 7d). Consequently, remote surface conditions are important in determining high temperatures near the surface in western Russia. The smallest influence of surface sensible heat fluxes is visible for trajectories arriving in the British Isles (blue line in Figure 8b). Both the daily magnitude and the number of days with notable surface fluxes is decreased compared with the other regions. Although some trajectories in cluster B_{sd} reaching the British Isles are located above parts of Germany, Denmark, Poland, and the Netherlands (Figure 7a), the influence of surface sensible heat fluxes over these countries is negligible and local surface heating over the British Isles is more important. Surface fluxes for Central Europe are in between the two mentioned cases, that is, increased surface fluxes five days before arrival, with a median maximum daily heating around 125 W/m^2 (Figure 8b). As shown in Figure 7c, most air parcels of clusters B_{sd} and B_{wd} are already located over Central Europe three days prior to the heat waves, highlighting the importance of local soil conditions and in situ warming, in agreement with Bieli *et al.* (2015). The Iberian Peninsula shows a similar temporal development of the surface sensible heat fluxes to the British Isles, but higher in magnitude (not shown). Because most of the trajectories are situated above the Mediterranean Sea and the Gulf of Biscay three days before the heat waves in the Iberian Peninsula (Figure 7e), the influence of surface fluxes is only present one to two days before the events. Surface sensible heat fluxes for Greece/Italy are similar to those for western Russia, and for Scandinavia they are similar to those for Central Europe, but trajectories for Greece/Italy and Scandinavia experience lower absolute surface fluxes (not shown). However, an interesting feature emerges for the position of the three clusters three days before the heat waves in Greece/Italy (Figure 7f). While cluster A is located mostly in the western half or slightly west of the target area, cluster B_{sd} and B_{wd} trajectories are also located to the northeast of Greece/Italy. Remote surface conditions are therefore important for high near-surface temperatures in Greece/Italy, similar to western Russia. Hence, not only local but also remote surface conditions seem to play an important role in establishing high surface temperatures for some regions in Europe.

The evolution of the relative and specific humidity of air parcels for the two contrasting regions of western Russia and the British Isles is depicted in Figure 9. Specific humidities near the origin of clusters A and B_{sd} are low, with values of about 2 g/kg (Figure 9b), due to the high altitudes. Throughout the descent, specific humidity increases steadily up to values around 8 g/kg. Due to the location in the lower troposphere, specific humidities of cluster B_{wd} are considerably higher and reveal a diurnal cycle for trajectories arriving in western Russia (Figure 9b). This strong diurnal cycle is not found for trajectories in cluster A, because they are located at higher altitudes. Compared with the specific humidity, the diurnal cycle is more pronounced for the relative humidity, due to the higher correlation with temperature. Although the specific humidity increases, the relative humidity decreases substantially, especially during the second half of the trajectories (Figure 9a). This highlights the pronounced warming during the last days, as mentioned by Santos *et al.* (2015) for heat waves in the Iberian Peninsula. The strong reduction of relative humidity is marked for clusters B_{sd} and B_{wd} and stronger for western Russia compared with the British Isles.

To summarize, most of the trajectories are already in the target regions three days prior to their arrival. Additionally, not only local but also remote surface conditions are important in determining high temperatures near the surface. Interestingly, the origins of air parcels forming a heat wave are very diverse. The geographic origin—and therefore the original temperature—is of minor importance. Rather more important are the pathway and the processes, that is, vertical motion and diabatic heating, along the trajectories. In all regions, three air streams with different thermodynamic characteristics and vertical motions converge in the heat wave regions: (a) air parcels originating from pressure levels around 600 hPa with temperatures mostly below freezing level, which are warmed due to subsidence only (cluster A), (b) air parcels

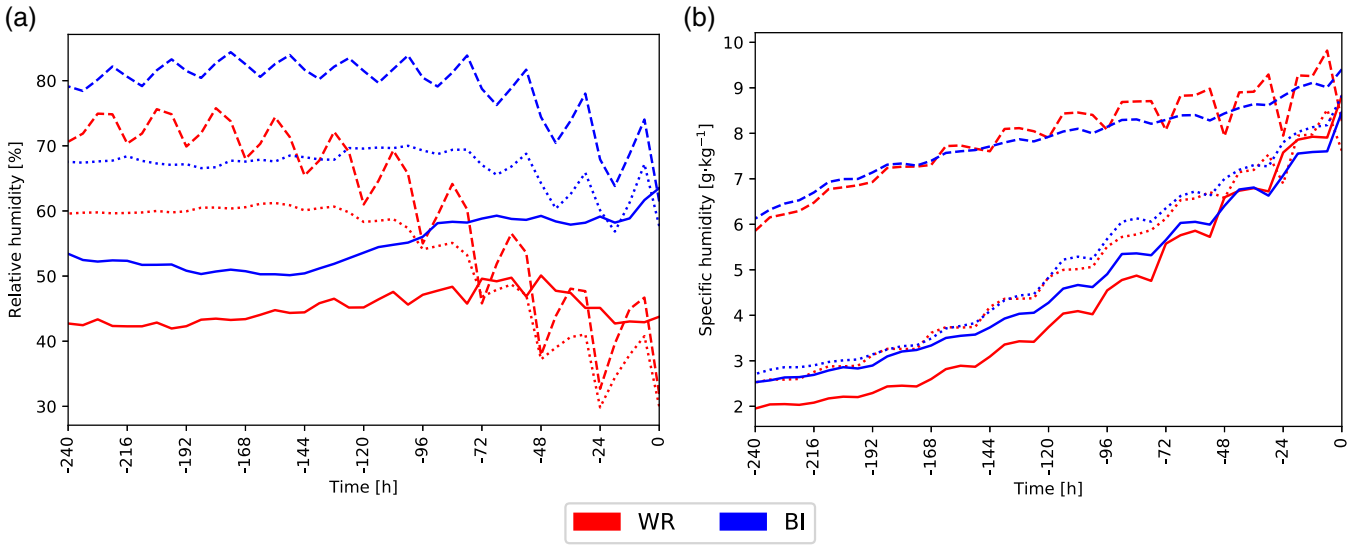

FIGURE 9 Temporal evolution of (a) median relative humidity and (b) specific humidity for heat wave trajectories from the British Isles (BI) and western Russia (WR). Solid lines: trajectory cluster *A*; dotted lines: B_{sd}; dashed lines: B_{wd}

originating from around 750 hPa, experiencing subsidence in the first eight days and being strongly heated diabatically near the surface in the last two days (cluster B_{sd}), and (c) air parcels located in the lower troposphere during the whole 10-day period that are strongly influenced by surface sensible heat fluxes (cluster B_{wd}).

3.5 | Quantification of processes

In order to quantify the most dominant process contributing to heat waves, we derive the horizontal temperature advection at 850 hPa for all heat wave days and the daily temperature change of air parcels due to vertical motion and diabatic processes for the three clusters (Lagrangian processes). The latter two processes were quantified following Bieli *et al.* (2015, their equation 1).

Figure 10 depicts temperature increases for the three trajectory clusters and two time periods: (a) 72 hr (3 days) prior to the arrival of the air parcels in the target area (Figure 10a–c) and (b) between 10 and three days prior to their arrival (Figure 10d–f). This separation is motivated by Bieli *et al.* (2015), because they determined that extreme temperature events develop on a two- to three-day time-scale.

Adiabatic warming due to vertical motion is much stronger than diabatic processes for the air parcels in cluster *A* (Figure 10a,d). The mean diabatic cooling rates between 10 and three days before the heat waves are around −1 K/day (Figure 10d), which is common for radiative cooling (e.g., Wallace and Hobbs, 2006). The warming due to subsidence increases strongly 72 hr before extreme events, with a maximum over the Iberian Peninsula of around 5 K/day in the mean and even up to 8 K/day along individual trajectories. The least warming due to subsidence occurs for the British Isles (around 3 K/day). Although the warming due to subsidence appears to be modest for the British Isles, it has been shown before that cluster *A* contains the largest fraction of trajectories for this region (Figure 6b).

Air parcels in cluster B_{sd} are mainly warmed due to adiabatic processes in the first seven days (Figure 10e). However, the influence of diabatic processes, that is, surface sensible heat fluxes, increases 72 hr before the heat waves (Figure 10b). Therefore the temperature increase 72 hr before the heat waves is due to subsidence and diabatic warming in equal parts, at a rate of about +1.5 K/day each.

In cluster B_{wd}, the daily temperature increase is comparably weak in the first seven days, due to the weak subsidence and diabatic warming (Figure 10f). Thus, those air parcels are transported near the surface without any notable temperature changes. However, 72 hr before the heat events, the diabatic warming increases greatly, especially over the Iberian Peninsula at a rate of about +4K per day, sometimes even up to 6 K/day (Figure 10c). Interestingly, air parcels typically ascend during this period, which may be induced by a heat low that establishes during extremely high temperatures over the Iberian peninsula (Santos *et al.*, 2015). Due to the ascent, air parcels cool adiabatically by up to −2 K/day, but, due to the strong diabatic warming near the surface, the warming of the air parcels predominates.

The third process, namely horizontal temperature advection, is illustrated in Figure 11. The Eulerian horizontal temperature advection $\boldsymbol{v} \cdot \boldsymbol{\nabla}_h T$ is calculated at a pressure level of 850 hPa at grid points that are affected by a heat wave. For calculating the temperature advection, we use all available time steps from ERA-Interim at 0000, 0600, 1200, and 1800 UTC. Figure 11 shows that, although some warm-air advection occurs for the British Isles and western Russia, generally, local horizontal temperature advection is not important

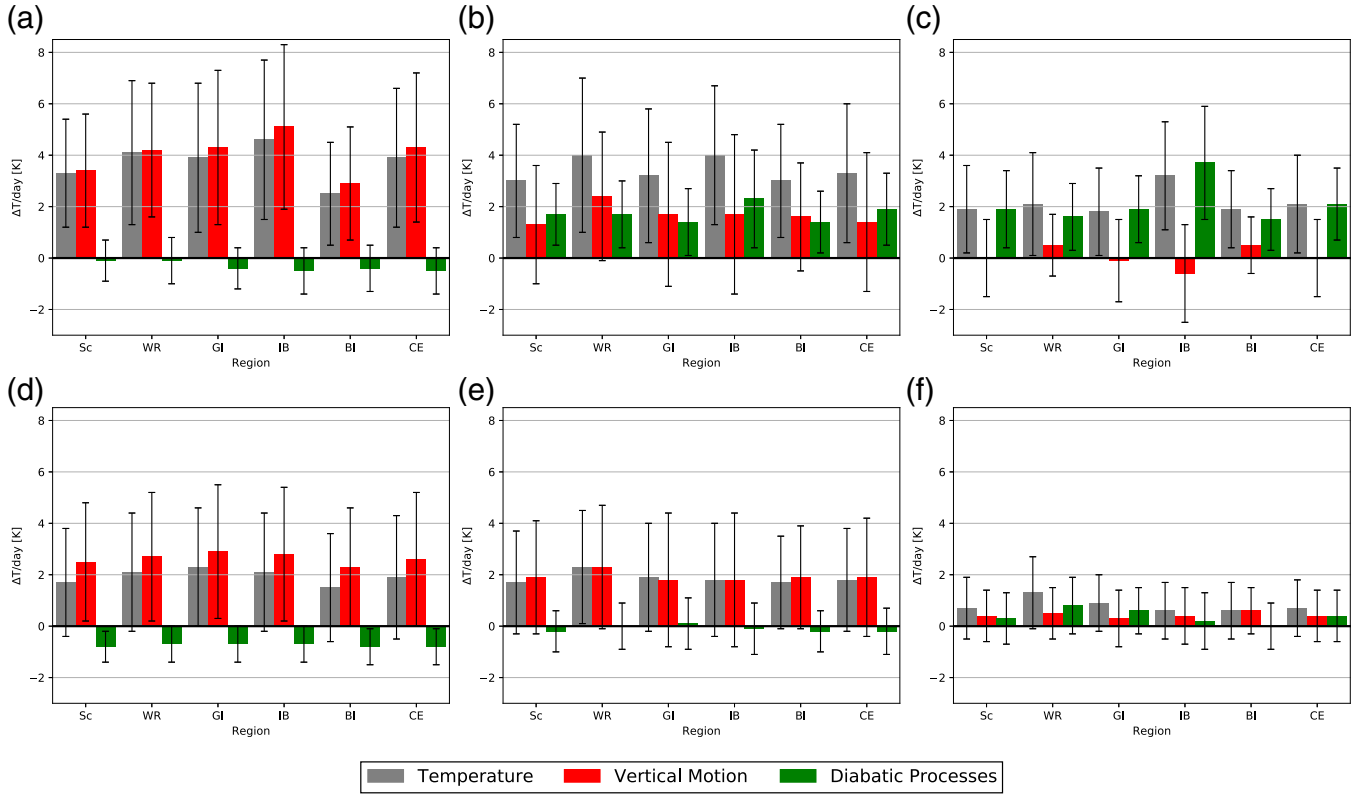

FIGURE 10 Daily Lagrangian temperature changes in K (grey: total temperature tendency, red: adiabatic temperature change due to vertical motion, green: diabatic temperature changes) for Scandinavia (Sc), western Russia (WR), Greece/Italy (GI), Iberian Peninsula (IB), British Isles (BI), and Central Europe (CE). Top row: temperature changes three days before the heat waves; bottom row: temperature changes between day 10 and 3 before the heat waves. Left: trajectory cluster *A*; middle: trajectory cluster B_{sd}; right: trajectory cluster B_{wd}. The bars denote the mean, the errors bars the standard deviation

in elevating near-surface temperatures during heat waves. The warm-air advection over the British Isles may be related to the fact that the ridge axis is not located exactly above the region (Figure 5f). This is also the reason why some air parcels originate from the west and southwest (Figure 7a). However, comparing the temperature tendencies between the advection and the two Lagrangian processes, it is obvious that the latter are pivotal.

3.6 | Residence time of air parcels

In order to quantify how long the air parcels, which lead to the high near-surface temperatures, are stalled in the target region (circles with 500 km radius as described in section 2.2), we calculate forward trajectories for the heat waves and determine when the trajectories exited the region. The longer the air parcels are located in the lower troposphere, the higher the potential influence of land–atmospheric feedbacks. During mega-heat waves, previous studies suggested that the heat can be stored over several days, resulting in a progressive accumulation of heat (Miralles *et al.*, 2014). The authors highlighted the multiday memory of land-surface feedbacks in the planetary boundary layer. With the help of forward trajectories, we try to quantify how often trajectories are being trapped in the heat wave area for multiple days. Figure 12 shows the residence time of the trajectories. The shortest (median) residence time is found for western Russia and the British Isles, while the longest is found for Central Europe and Scandinavia (around 1.5 days). Although there are also cases of longer residence times in all regions, most of the trajectories are in the target region between 0.5 and 2.5 days only. Due to the minimum duration of three days for heat waves, air masses are therefore steadily descending into the heat wave areas (presumably trajectory cluster *A*) or transported horizontally from adjacent regions (presumably trajectory clusters B_{sd} and B_{wd}). Hence, hot air masses are mostly not stagnant over a time period longer than a few days. For the extreme heat waves in Central Europe in 2003 and western Russia in 2010, we found similar median residence times of 30 hr for Central Europe (Figure S8) and 24 hr for western Russia (Figure S9), underlying the importance of the Lagrangian processes mentioned above. It is generally possible that air parcels can re-enter the target area after exiting the region, which may happen in a blocking anticyclone with recirculating air masses. About 10–15% of the trajectories re-enter the target area within a 10-day period. Hence, although the synoptic pattern is nearly stationary during heat wave periods due to the low variability of the associated ridges above the

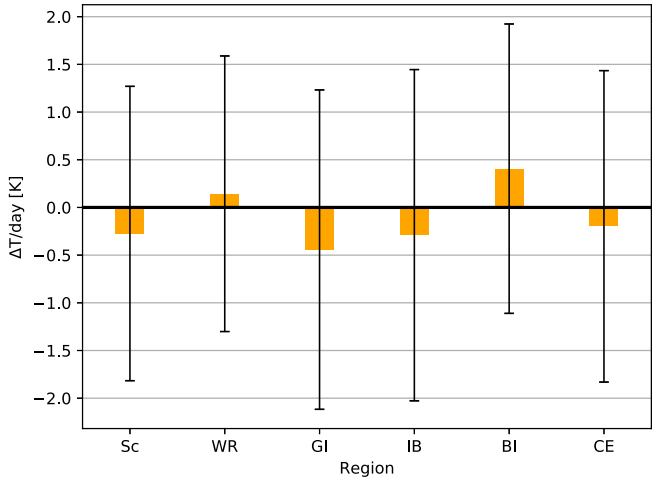

FIGURE 11 Horizontal temperature advection at 850 hPa at 0000, 0600, 1200, and 1800 UTC for heat waves in Scandinavia (Sc), western Russia (WR), Greece/Italy (GI), Iberian Peninsula (IB), British Isles (BI), and Central Europe (CE). The bars denote the mean, the error bars the standard deviation

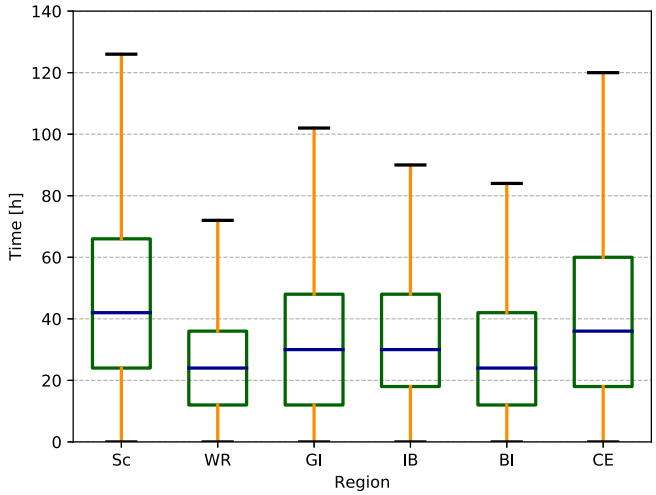

FIGURE 12 Residence time of trajectories in the target regions for heat waves in Scandinavia (Sc), western Russia (WR), Greece/Italy (GI), Iberian Peninsula (IB), British Isles (BI), and Central Europe (CE). The blue lines depict the median, the boxes the interquartile range (IQR) and the whiskers 1.5 times the interquartile range

areas (Figure 5), the involved air masses leading to extreme temperatures are mostly not stationary. In that sense, new air masses that experience subsidence in the free atmosphere and diabatic heating near the surface replace the old air mass.

4 | CONCLUSIONS AND OUTLOOK

In this study, we presented a comprehensive analysis of processes determining heat waves across European regions representing different climates for the period 1979–2016. Heat waves were defined using the percentile-based HWMId (Russo *et al.*, 2015). We investigated different statistical properties of heat waves (frequencies and duration), their associated synoptic patterns, and analysed the physical processes along trajectories that led to high near-surface temperatures. The processes quantified along the trajectories were adiabatic warming by subsidence and diabatic processes. This quantification was complemented by an Eulerian calculation of horizontal temperature advection.

Heat waves persist for four to five days and occur usually once or twice per year. Upper-level ridges accompany high surface temperatures, corroborating the findings of Pfahl and Wernli (2012) and Sousa *et al.* (2018). The amplitudes of the ridges are generally lower in Greece/Italy and the Iberian Peninsula compared with Scandinavia. Upstream of the ridges, the amplitudes of the troughs over the North Atlantic Ocean are highly variable.

Horizontal transport of (already) warm air, that is, temperature advection, appears not to be an important factor in establishing heat waves. In contrast, subsidence, entrainment of warm air into the lower troposphere, and diabatic heating due to surface sensible heat fluxes are crucial in determining high temperatures near the surface. This corroborates the findings of Bieli *et al.* (2015). In all regions, three trajectory clusters are associated with high near-surface temperatures. All these clusters experience an increase in the temperature of air parcels, however, with differences in diabatic heating and vertical motions (see Table 1 for the definition of the clusters). The increase of temperatures of the trajectories is accelerated in the last three days prior to the heat waves. Most of the trajectories are already near to or in the target area three days prior to the heat waves. The trajectory cluster *A* is overall diabatically cooled due to radiative cooling in the free atmosphere. During the last three days, air parcels in this cluster are strongly descending in the vicinity of the heat wave area, leading to a heating rate of between 3 and 5 K per day. Cluster B_{sd} experiences overall diabatic heating and descends strongly. In the last three days, the warming of the air parcels is due to both subsidence (1.5 K per day) and surface fluxes (1.5 K per day). The third cluster, B_{wd}, is located near the surface and diabatically heated at a rate of about 2 K/day, with a maximum for the Iberian Peninsula of about 4 K/day three days before a heat wave.

About 50% of all trajectories fall into cluster B_{sd} and 25% fall into clusters *A* and B_{wd}, respectively, with some interregional differences. Although subsidence is a very important driving factor, surface sensible heat fluxes are also important for western Russia, whereas the British Isles are less influenced by surface fluxes. With respect to the role of diabatic heating near the surface, in addition to the local influence of surface sensible heat fluxes, for example in western Russia, remote surface fluxes in regions to the east of the target region also play an important role. Similar results are found for Greece/Italy, where the influence of surface fluxes to the

northeast is also important. Quinting and Reeder (2017) found a similar result for heat waves in southeastern Australia. They argued that local effects of soil moisture are of minor importance, whereas transport above remote dry soils has a larger impact. The inflow of heat and moisture from remote regions to the heat wave area was named "event self-propagation" by Miralles *et al.* (2019), and seems to be important for western Russia and to a lesser extent for Greece/Italy. However, as noted by Miralles *et al.* (2019), these remote interactions are still not well understood and provide avenues for further research. Throughout the life cycle of a heat wave, new air masses are imported steadily into the heat wave regions, due to either subsidence from higher levels or air coming from adjacent areas heated by surface fluxes. Our results therefore suggest that the Lagrangian processes discussed are crucial in determining the high near-surface temperatures, whereas the stagnation of air masses for longer than a few days is of minor importance for European heat waves. Stagnant air masses are more important for air parcels in cluster B_{wd}, which are located in the target area near the surface and are diabatically heated with nearly no vertical motion.

Our analysis reveals that pure horizontal temperature advection of already warm air is not important for creating high near-surface temperatures in the European regions considered. A similar result was found by Quinting and Reeder (2017) for heat waves in Australia. Our result is likely influenced by our heat wave definition, because we exclude heat episodes below three days duration. Shorter heat episodes can be a result of horizontal temperature advection ahead of an upper-level trough near an extratropical cyclone. In such a situation, warm-air advection may be able to elevate temperatures near the surface for one day; however, the passage of the cyclone's cold front typically leads to a temperature decrease shortly after. Additionally, the impact of such short heat periods is comparably small. An important process not considered in this study is the formation of ridges. A study focusing on southeastern Australia analysed this systematically and highlighted the importance of cloud–diabatic processes that are responsible for the formation and maintenance of the ridge (Quinting and Reeder, 2017). Focusing on blocking systems in general, Pfahl *et al.* (2015) emphasized the importance of latent heat release in the formation of blocking, in addition to the isentropic advection of low potential vorticity air. It would therefore be worth studying the formation of ridges that accompany European heat waves. Additionally, it would be interesting to find cases in which the large-scale setting (i.e., ridge) is conducive to a heat wave, but the surface temperatures were not high. A comparison of the Lagrangian processes leading to heat waves in other areas (e.g., Tropics, polar regions) would complete the analysis presented in this study.

Given the importance of heat waves, due to their manifold impacts (WMO and WHO, 2015), it is crucial that the processes described in our study are modelled correctly in state-of-the-art weather forecasting and climate models. For example, the Lagrangian trajectory analysis presented here may be applied to an ensemble forecasting system to assess why some ensemble members perform better or worse. Furthermore, climate models can have systematic errors in simulating specific weather patterns, for example, blocking (Sillmann *et al.*, 2017). It is therefore worth applying the Lagrangian framework to climate models and quantifying the contributions of diabatic heating near the surface and subsidence to the formation of high near-surface temperature extremes in different parts of the globe in a warmer climate.

Our results imply that future changes in heat waves, over and above the background thermodynamic warming, may be affected by potential changes in the associated dynamical processes, in particular the strength of the subsidence. In addition, our results suggest that "event-self propagation" may be important for western Russia and, to a lesser extent, Greece/Italy. Overall, the results of the present study provide a guideline as to which processes and diagnostics weather and climate studies could focus on to understand the severity of heat waves.

ACKNOWLEDGEMENTS

We thank ECMWF for providing access to ERA-Interim reanalysis data, as well as Christian Grams and Julian Quinting for inspiring discussions. The research leading to these results has been conducted within the subproject C4: Coupling of planetary-scale Rossby-wave trains to local extremes in heat waves over Europe of the Transregional Collaborative Research Center SFB/TRR 165 "Waves to Weather", funded by the German Research Foundation (DFG). We thank two anonymous reviewers for their helpful feedback on the manuscript.

REFERENCES

Alexander, L. (2011) Extreme heat rooted in dry soils. *Nature Geoscience*, 4, 12–13.

Bieli, M., Pfahl, S. and Wernli, H. (2015) A Lagrangian investigation of hot and cold temperature extremes in Europe. *Quarterly Journal of the Royal Meteorological Society*, 141, 98–108.

Binder, H., Boettcher, M., Grams, C.M., Joos, H., Pfahl, S. and Wernli, H. (2017) Exceptional air mass transport and dynamical drivers of an extreme wintertime Arctic warm event. *Geophysical Research Letters*, 44, 12028–12036.

Boschat, G., Pezza, A., Simmonds, I., Perkins, S., Cowan, T. and Purich, A. (2015) Large scale and sub-regional connections in the lead up to summer heat wave and extreme rainfall events in eastern Australia. *Climate Dynamics*, 44, 1823–1840.

Carlson, T.N. (1994) *Mid-latitude Weather Systems* p. 507. New York: Routledge.

Cassou, C., Terray, L. and Phillips, A.S. (2005) Tropical Atlantic influence on European heatwaves. *Journal of Climate*, 18, 2805–2811.

Collins, M., Knutti, R., Arblaster, J., Dufresne, J.-L., Fichefet, T., Friedlingstein, P., Gao, X., Gutowski, W., Johns, T., Krinner, G., Shongwe, M., Tebaldi, C., Weaver, A. and Wehner, M. (2013) Long-term climate change: projections, commitments and irreversibility. In: Stocker, T.F., Qin, D., Plattner, G.-K., Tignor, M., Allen, S.K., Boschung, J., Nauels, A., Xia, Y., Bex, V. and Midgley, P.M. (Eds.) *Climate Change 2013: The Physical Science Basis. Contribution of Working Group I to the Fifth Assessment Report of the Intergovernmental Panel on Climate Change*. Cambridge, UK and New York, NY: Cambridge University Press, pp. 1029–1136.

Dee, D.P., Uppala, S.M., Simmons, A.J., Berrisford, P., Poli, P., Kobayashi, S., Andrae, U., Balmaseda, M.A., Balsamo, G., Bauer, P., Bechtold, P., Beljaars, A.C., van de Berg, L., Bidlot, J., Bormann, N., Delsol, C., Dragani, R., Fuentes, M., Geer, A.J., Haimberger, L., Healy, S.B., Hersbach, H., Hólm, E.V., Isaksen, L., Kållberg, P., Köhler, M., Matricardi, M., Mcnally, A.P., Monge-Sanz, B.M., Morcrette, J.J., Park, B.K., Peubey, C., de Rosnay, P., Tavolato, C., Thépaut, J.N. and Vitart, F. (2011) The ERA-Interim reanalysis: configuration and performance of the data assimilation system. *Quarterly Journal of the Royal Meteorological Society*, 137, 553–597.

Fink, A.H., Brucher, T., Kruger, A., Leckebusch, G.C., Pinto, J.G. and Ulbrich, U. (2004) The 2003 European summer heat waves and drought – synoptic diagnosis and impact. *Weather*, 59, 209–216.

Fischer, E.M. and Schär, C. (2010) Consistent geographical patterns of changes in high-impact European heatwaves. *Nature Geoscience*, 3, 398–403.

Fischer, E.M., Seneviratne, S.I., Lüthi, D. and Schär, C. (2007) Contribution of land–atmosphere coupling to recent European summer heat waves. *Geophysical Research Letters*, 34, L06707.

Fragkoulidis, G., Wirth, V., Bossmann, P. and Fink, A.H. (2018) Linking Northern Hemisphere temperature extremes to Rossby wave packets. *Quarterly Journal of the Royal Meteorological Society*, 144, 553–566.

Grumm, R.H. (2011) The Central European and Russian heat event of July–August 2010. *Bulletin of the American Meteorological Society*, 92, 1285–1296.

Hirschi, M., Seneviratne, S.I., Alexandrov, V., Boberg, F., Boroneant, C., Christensen, O.B., Formayer, H., Orlowsky, B. and Stepanek, P. (2011) Observational evidence for soil-moisture impact on hot extremes in southeastern Europe. *Nature Geoscience*, 4, 17–21.

Horton, R.M., Mankin, J.S., Lesk, C., Coffel, E. and Raymond, C. (2016) A review of recent advances in research on extreme heat events. *Current Climate Change Reports*, 2, 242–259.

Lee, Y.Y. and Grotjahn, R. (2016) California Central Valley summer heat waves form two ways. *Journal of Climate*, 29, 1201–1217.

Messori, G., Caballero, R., Bouchet, F., Faranda, D., Grotjahn, R., Harnik, N., Jewson, S., Pinto, J.G., Rivière, G., Woollings, T. and Yiou, P. (2018) An interdisciplinary approach to the study of extreme weather events: large-scale atmospheric controls and insights from dynamical systems theory and statistical mechanics. *Bulletin of the American Meteorological Society*, 99, ES81–ES85.

Miralles, D.G., Gentine, P., Seneviratne, S.I. and Teuling, A.J. (2019) Land-atmospheric feedbacks during droughts and heatwaves: state of the science and current challenges. *Annals of the New York Academy of Sciences*, 1436, 19–35.

Miralles, D.G., Teuling, A.J., Van Heerwaarden, C.C. and De Arellano, J.V.G. (2014) Mega-heatwave temperatures due to combined soil desiccation and atmospheric heat accumulation. *Nature Geoscience*, 7, 345–349.

MunichRe (2018) *TOPICS GEO Natural Catastrophes 2017*. Munich: Münchener Rückversicherungs-Gesellschaft. p. 68. Available at: https://www.munichre.com/site/touch-publications/get/documents_E711248208/mr/assetpool.shared/Documents/5_Touch/_Publications/TOPICS_GEO_2017-en.pdf [Accessed 17th June 2019]

Perkins, S.E. (2015) A review on the scientific understanding of heatwaves – their measurement, driving mechanisms, and changes at the global scale. *Atmospheric Research*, 164–165, 242–267.

Perkins, S.E., Alexander, L.V. and Nairn, J.R. (2012) Increasing frequency, intensity and duration of observed global heatwaves and warm spells. *Geophysical Research Letters*, 39, L20714.

Petoukhov, V., Rahmstorf, S., Petri, S. and Schellnhuber, H.J. (2013) Quasiresonant amplification of planetary waves and recent Northern Hemisphere weather extremes. *Proceedings of the National Academy of Sciences of the United States of America*, 110, 5336–5341.

Pfahl, S. (2014) Characterising the relationship between weather extremes in Europe and synoptic circulation features. *Natural Hazards and Earth System Sciences*, 14, 1461–1475.

Pfahl, S., Schwierz, C., Croci-Maspoli, M., Grams, C.M. and Wernli, H. (2015) Importance of latent heat release in ascending air streams for atmospheric blocking. *Nature Geoscience*, 8, 610–614.

Pfahl, S. and Wernli, H. (2012) Quantifying the relevance of atmospheric blocking for colocated temperature extremes in the Northern Hemisphere on (sub-)daily time scales. *Geophysical Research Letters*, 39, L12807.

Quandt, L.-A., Keller, J.H., Martius, O. and Jones, S.C. (2017) Forecast variability of the blocking system over Russia in Summer 2010 and its impact on surface conditions. *Weather and Forecasting*, 32, 61–82.

Quinting, J.F. and Reeder, M.J. (2017) Southeastern Australian heat waves from a trajectory viewpoint. *Monthly Weather Review*, 145, 4109–4125.

Raveh-Rubin, S. (2017) Dry intrusions: Lagrangian climatology and dynamical impact on the planetary boundary layer. *Journal of Climate*, 30, 6661–6682.

Röthlisberger, M., Pfahl, S. and Martius, O. (2016) Regional-scale jet waviness modulates the occurrence of midlatitude weather extremes. *Geophysical Research Letters*, 43, 10989–10997.

Russo, S., Sillmann, J. and Fischer, E.M. (2015) Top ten European heatwaves since 1950 and their occurrence in the coming decades. *Environmental Research Letters*, 10, 124003.

Santos, J.A., Pfahl, S., Pinto, J.G. and Wernli, H. (2015) Mechanisms underlying temperature extremes in Iberia: a Lagrangian perspective. *Tellus, Series A: Dynamic Meteorology and Oceanography*, 67, 26032.

Schaller, N., Sillmann, J., Anstey, J., Fischer, E.M., Grams, C.M. and Russo, S. (2018) Influence of blocking on Northern European and Western Russian heatwaves in large climate model ensembles. *Environmental Research Letters*, 13, 054015.

Seneviratne, S.I., Nicholls, N., Easterling, D., Goodess, C.M., Kanae, S., Kossin, J., Luo, Y., Marengo, J., McInnes, K., Rahimi, M., Reichstein, M., Sorteberg, A., Vera, C. and Zhang, X. (2012) Changes in climate extremes and their impacts on the natural physical environment. In: Field, C.B., Barros, V., Stocker, T.F., Qin, D., Dokken, D.J., Ebi, K.L., Mastrandrea, M.D., Mach, K.J., Plattner, G.-K., Allen, S.K., Tignor, M. and Midgley, P.M. (Eds.) *Managing the Risks of Extreme Events and Disasters to Advance Climate Change*

Adaptation. A Special Report of Working Groups I and II of the Intergovernmental Panel on Climate Change (IPCC). Cambridge, UK, and New York, NY: Cambridge University Press, pp. 109–230.

Sillmann, J., Thorarinsdottir, T., Keenlyside, N., Schaller, N., Alexander, L.V., Hegerl, G., Seneviratne, S.I., Vautard, R., Zhang, X. and Zwiers, F.W. (2017) Understanding, modeling and predicting weather and climate extremes: challenges and opportunities. *Weather and Climate Extremes*, 18, 65–74.

Sousa, P.M., Trigo, R.M., Barriopedro, D., Soares, P.M.M. and Santos, J.A. (2018) European temperature responses to blocking and ridge regional patterns. *Climate Dynamics*, 50, 457–477.

Sprenger, M. and Wernli, H. (2015) The LAGRANTO Lagrangian analysis tool – Version 2.0. *Geoscientific Model Development*, 8, 2569–2586.

Stefanon, M., Dandrea, F. and Drobinski, P. (2012) Heatwave classification over Europe and the Mediterranean region. *Environmental Research Letters*, 7, 014023.

Tyrlis, E. and Hoskins, B.J. (2008) Aspects of a Northern Hemisphere atmospheric blocking climatology. *Journal of the Atmospheric Sciences*, 65, 1638–1652.

Wallace, J.M. and Hobbs, P.V. (2006) *Atmospheric Science: An Introductory Survey*, Vol. 504. Amsterdam: Elsevier Academic Press.

Wirth, V., Riemer, M., Chang, E.K.M. and Martius, O. (2018) Rossby wave packets on the midlatitude waveguide – a review. *Monthly Weather Review*, 146, 1965–2001.

WMO and WHO. (2015) *Heatwaves and Health: Guidance on Warning-System Development*. No. 1142, 114 pp. Geneva: World Meteorological Organization and World Health Organization. Available at:. http://www.who.int/globalchange/publications/WMO_WHO_Heat_Health_Guidance_2015.pdf [Accessed 8th July 2019].

Woollings, T., Barriopedro, D., Methven, J., Son, S.-W., Martius, O., Harvey, B., Sillmann, J., Lupo, A.R. and Seneviratne, S. (2018) Blocking and its response to climate change. *Current Climate Change Reports*, 4, 287–300.

Xu, Z., FitzGerald, G., Guo, Y., Jalaludin, B. and Tong, S. (2016) Impact of heatwave on mortality under different heatwave definitions: a systematic review and meta-analysis. *Environment International*, 89–90, 193–203.

Zschenderlein, P., Fragkoulidis, G., Fink, A.H. and Wirth, V. (2018) Large-scale Rossby wave and synoptic-scale dynamic analyses of the unusually late 2016 heatwave over Europe. *Weather*, 73, 275–283.

SUPPORTING INFORMATION

Additional supporting information may be found online in the Supporting Information section at the end of this article.

How to cite this article: Zschenderlein P, Fink AH, Pfahl S, Wernli H. Processes determining heat waves across different European climates. *Q J R Meteorol Soc*. 2019;1–17. https://doi.org/10.1002/qj.3599